Stress-Strain Relations and Plastic Fatigue Phenomenon of Welded Beam-To-Column Connections

By

Kiyoshi KANETA and Isao KOHZU

(Received December 26, 1981)

Abstract

In order to examine the safety of steel structures against earthquakes, this paper deals with the stress-strain behavior and plastic fatigue strength of welded beam-to-column connections subjected to cyclic bending moments at relatively low cycles.

A number of cantilever type specimens were subjected to cyclic loadings at the tips of the beams in a manner which induced constant tip deflection amplitudes, until the specimens were fractured at the beam ends. The loads, deflections and strains, at or near the beam ends, were measured during the cyclic loadings.

From the test results, it was observed that local strains at or near the beam ends were distinctly influenced by the geometrical shapes of the beam ends, as well as by the thermal alteration due to welding.

The values of the low cycle fatigue strengths of the actual beam ends were predicted by using linear relations in a log-log scale between the averaged non-dimensional strain ranges at the beam ends and the lives at the fracture or the crack initiation lives. Then they were compared with those of JIS SS 41 base metals and the welded joints.

A remarkable deterioration of the fatigue strength was observed for the welded beam-to-column connections.

1. Introduction

In current structural design practices, it is generally agreed that a steel structure subjected to destructive earthquakes undergoes large cyclical deflections, which take the structural components beyond their elastic limits. Such considerations, inevitably require a method of estimating quantitatively aseismic safety, based upon the incidence of low cycle fatigue damage in the critical cross-sections of some members in the steel structure.

In the actual steel structure, the critical sections exist at the structural connections, sub-assemblages, and/or the structural elements. In particular, the welded beam-to-column connection comprises one of the most important sections in this regard. In

Department of Architectural Engineering

the so-called weak beam type connections, the heat-hardening of the welding process, and the stress concentrations caused by the scallops, or cope holes, which enhance the welding reliability and performance at the beam ends, ultimately contribute to the deterioration of the strength and ductility of these connections.

In the practical design of steel structures, Igarashi[1] recommended that careful attention should be paid to structural defects of welded beam-to-column connections arising from scalloping, which contributes to develop fatigue cracks, strength deteriorations, crack propagations, and brittle fracture.

Popov et al[2] tested beam-to-column connections to clarify the behavior of these components under cyclic loading by using cantilever type specimens of wholly welded connections, connections with butt-welded flanges and high tensile bolted webs. The results of the experiment showed a significant occurrence of fracture patterns, in which the crack of the beam flange initiated near, or from, a scallop or welded zone. Moreover, because of the strain concentration at the beam end, it was suggested that the load and tip deflection relations under cyclic loadings could be expressed by an analytical formula, taking into consideration the plastic hinges at the beam ends.

Another study[3] was made on a similar brittle fracture phenomenon initiating from the scallop at the beam flange.

However, to date, no investigations have quantitatively evaluated the deterioration of the fatigue strength at or near the beam ends. In this paper, the phenomena of the deterioration of the fatigue strength and the local strain behavior which occurs at or near the beam ends under cyclic loadings are discussed.

2. Specimens and Loading Apparatus

2.1 Specimens

Fig. 1 shows the shape and size of the test specimen. The beam flanges were single-bevel butt-welded to the column flange. Sections H-200×100×5.5×8 and H-200×200×8×12 were used for the beam and column, respectively. Both were made of JIS SS 41 steel. The beam web was fillet welded to the column flange. The web fillet at the beam ends was scalloped to 3.0 cm in radius so as to insure a good welding performance, and to simulate conditions in actual steel works. The specimens were classified into the following two types: Series 1 specimens were butt-welded with backing strip at the beam flanges to the column flanges.

Series 2 specimens were butt-welded with back run. The details of the groove shapes are illustrated in Fig. 2.

The welding was done by means of the manual arc welding. The web was first

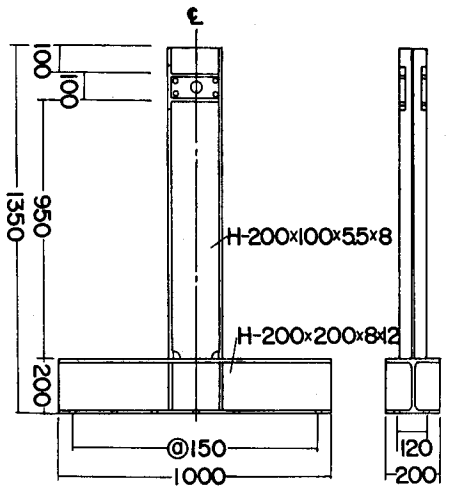

Fig. 1 Specimen (Unit: mm)

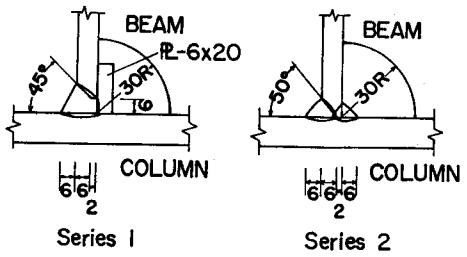

Fig. 2 Groove Shapes of the Beam Flanges (Unit: mm)

welded to the column flange and, after this, each flange was welded. An ultrasonic flaw test was conducted on all the welded specimens, and the test results did not show any significant weld defects.

2.2 Loading Apparatus and Measurement System

A special loading apparatus and the supporter are shown in Fig. 3. The specimen was mounted on the reaction frame and subjected to cyclic, plus and minus, bending moments generated by a hydraulic double action jack (with the capacity of 30 tons).

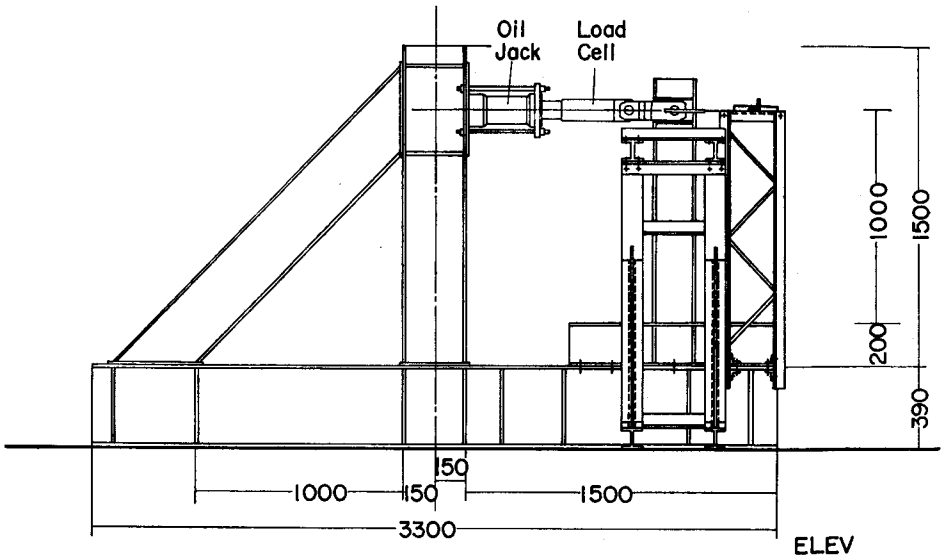

(3-a)

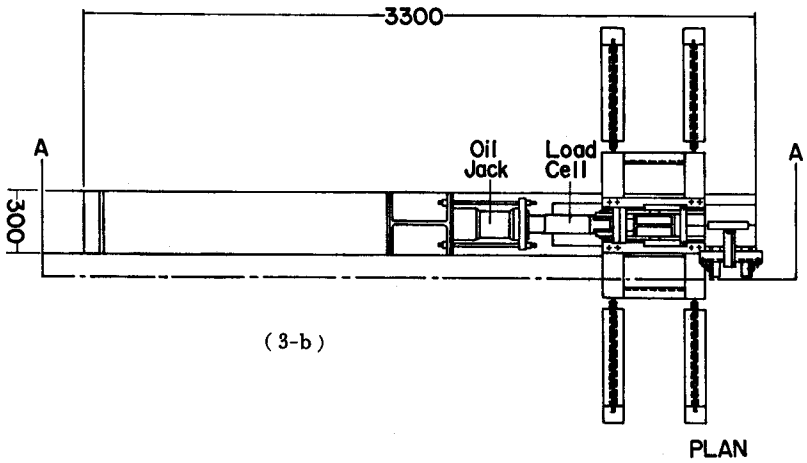

Fig. 3 General View of the Test Set-up (Unit: mm)

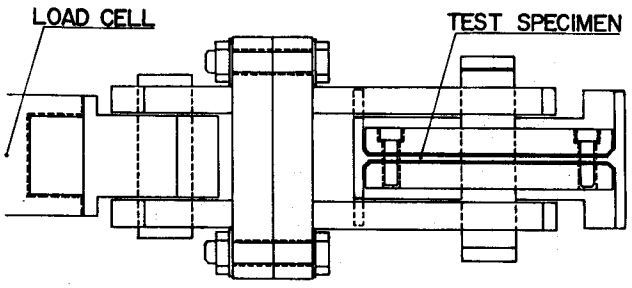

Fig. 4 Close-up of Joints

A load cell (transducer), directly connected to the oil jack at one end, was linked to the tip of the specimen at the other end by a pair of clevises held in place by pins, as shown in Fig. 4. A lateral guide frame was provided in order to arrest any lateral torsional buckling of the cantilever beam specimen during cyclic loading. The overall test equipment is shown in Figs. 5 (a) and (b).

The magnitude of the applied loads was monitored by the load cell (transducer), and the tip deflection of the cantilever beam was measured by an extensometer of the strain gauge type which was attached to the pin.
The data were plotted automatically on an X-Y recorder.

Fig. 6 shows the locations of the strain gauges at or near the beam ends. Local strains at or near the beam ends were monitored by a multichannel digital static strainmeter, and the outputs were recorded on a printer at the selected time intervals.

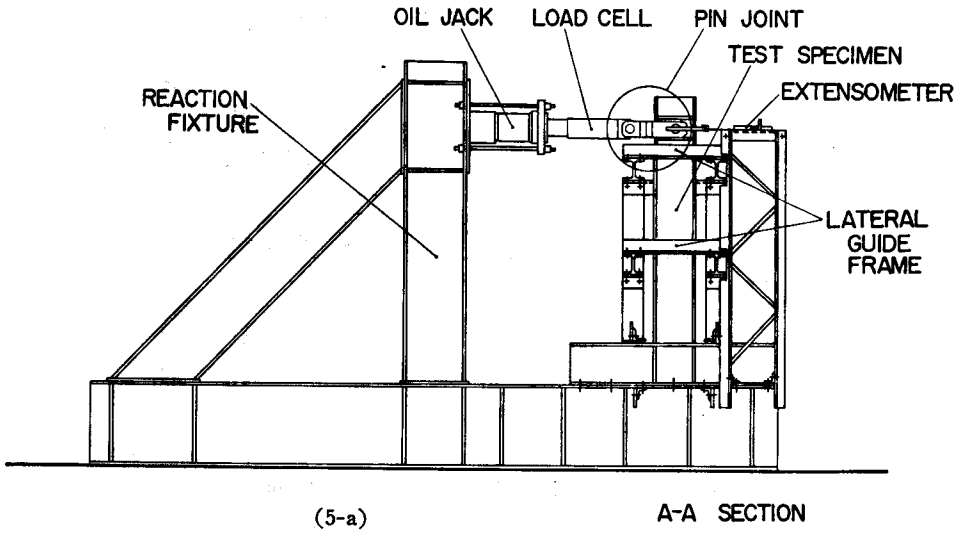

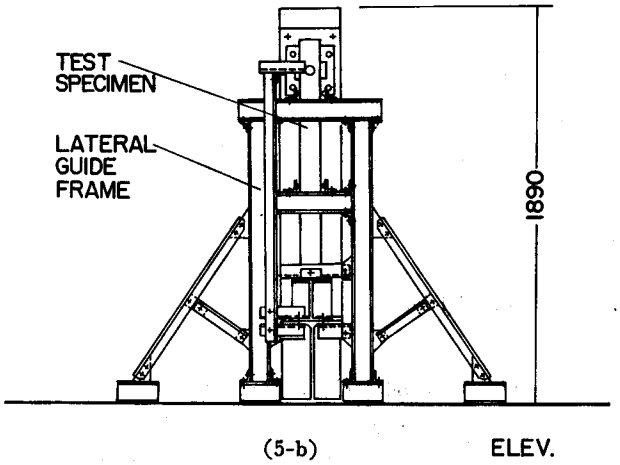

Fig. 5 Mounting Arrangement and Lateral Guide Frame

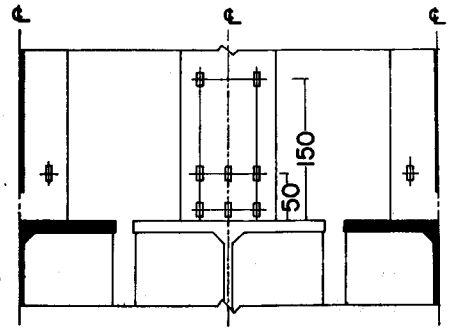

Fig. 6 Locations of the Strain Gauges

3. Experimental Procedure and Results

3.1 Monotonic Tensile Test

The mechanical properties of the rolled wide flange material are fundamentally related to the load carrying capacities of the beam, and were examined by the monotonic tensile test as follows. The stub of the beam was cut into three pieces, namely, the two flange plates and the web. Each plate was fabricated into the forms shown in Fig. 7. Each specimen was used for the monotonic tensile test, the results

Table 1 Mechanical Properties of the Base Metal

		Series 1		Series 2	
		Flange	Wed	Flange	Wed
σ_y : Yield Point	(kg/mm²)	27.8	30.9	35.2	39.6
ε_y : Yield Strain	(%)	0.13	0.145	0.162	0.205
σ_u : Tensile Strength	(kg/mm²)	41.0	44.8	48.7	47.5
δ : Elongation	(%)	27.8	28.3	28.4	20.8
E : Young's Modulus*	(kg/mm²)	2.14	2.13	2.17	1.93

* $\times 10^4$

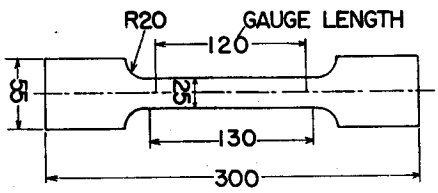

Fig. 7 Specimen used for the Monotonic Tensile Test (Unit: mm)

Table 2 Relations between the Selected Tip Deflections and the Resultant Fatigue Lives

δ (cm)	$N_f(N_c)$ (cycles) Series 1	Series 2
0.74	605(504)	—
1.00	189(130)	211(175)
1.26	53 (30)	94(70), 127(90)
1.52	—	50 (25)
1.78	—	39 (20)

of which are tabulated in Table 1.

3.2 Cyclic Loading Test

The cyclic load was applied at a selected tip deflection amplitude to the beam, and the test was terminated only after a perfect fracture occurred at the beam flange at or near the column flange. The selected tip deflection amplitude, the corresponding fatigue lives, and the crack initiation lives are tabulated in Table 2.

a) Cyclic Load and Tip Deffection Relations

The peak load values versus the corresponding number of cycles for every specimen are plotted as shown in Fig. 8. From this figure, it could be observed that, as a common tendency, the strain hardening initiates at the initial half cycle and terminates at the second cycle, and that the peak loads have their maximum (or minimum) values at these points.

When the selected tip deflection amplitudes are comparatively small, the subsequent peak loads follow the constant values until about 80 % of the lives to failure. However, when the amplitudes are large, the cyclic softening occurs as early as the third cycle. In the subsequent cycles, the greater the number of cycles, the smaller the peak loads. Namely, the strength deterioration due to cyclic loadings can be distinctly observed.

The cracks initiated at the intersection between the beam flange and the scallop,

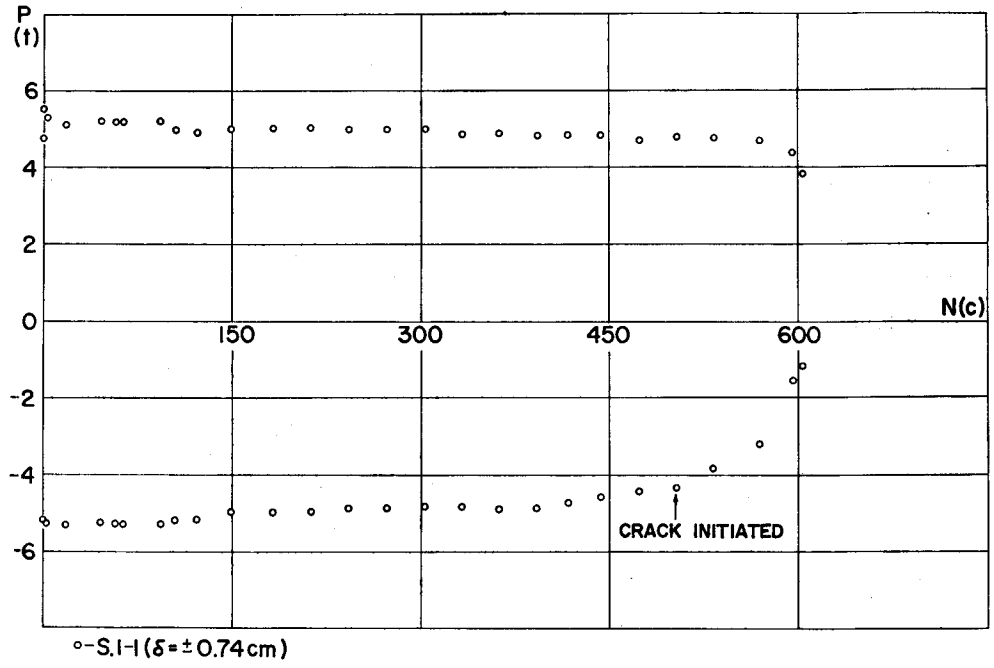
P
(t)
6
4
2
0
-2
-4
-6
150
300
450
600
N(c)
CRACK INITIATED
○-S.I-1 (δ=±0.74cm)

(8-a)

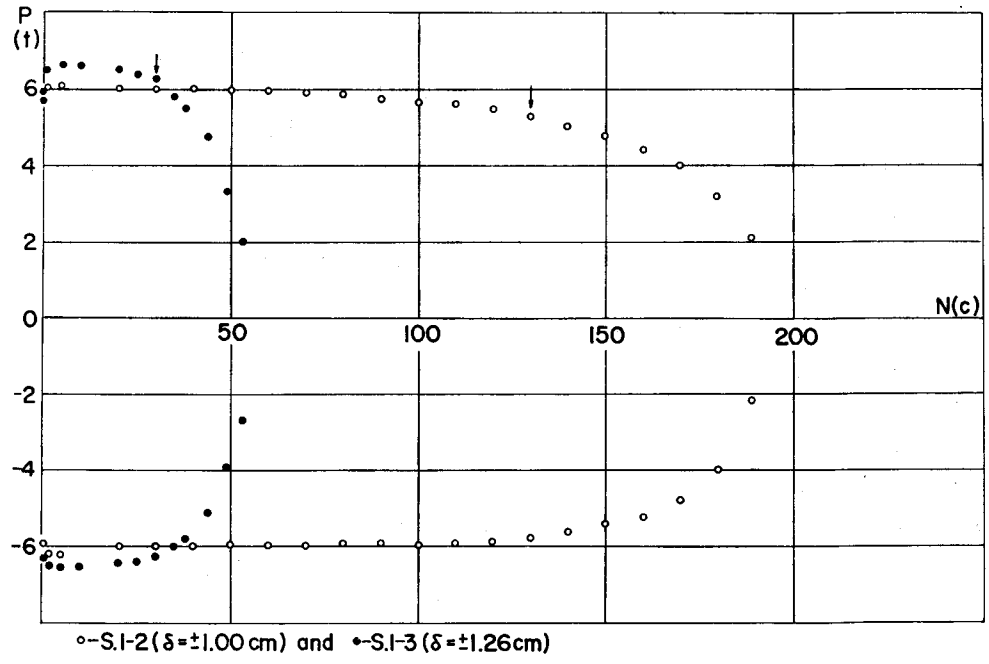
P
(t)
6
4
2
0
-2
-4
-6
50
100
150
200
N(c)
○-S.I-2 (δ=±1.00 cm) and •-S.I-3 (δ=±1.26cm)

(8-b)

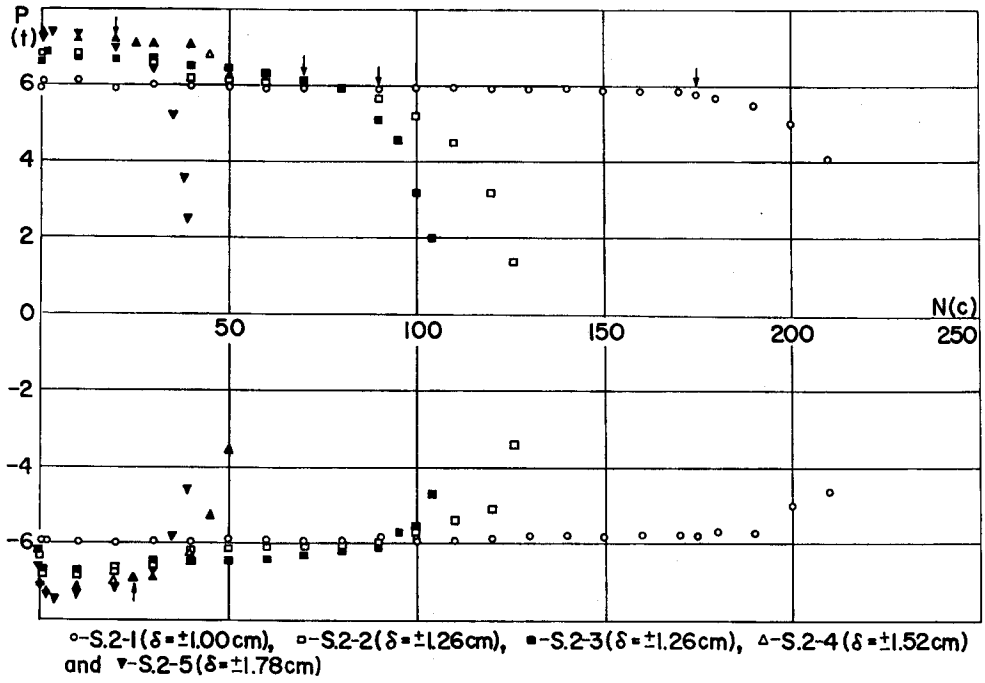

(8-c)

Fig. 8 Relations between the Peak Loads and the Cycles

or at the welded connection of the beam flange. They then spread along the cross sectional direction of the beam flange. As far as this experiment was concerned, neither local buckling behavior nor any brittle fracture at the beam end could be observed, even though the degrees of deterioration of the peak loads differed from each other.

The crack initiation life observed at the beam flange with the naked eye is shown in Fig. 8, with the symbol ↓. Attention should be paid to the fact that the crack initiation can be invariably found at the cycle where the peak load is below that of the initial state.

The above characteristics were independent of the shapes of the two kinds of test specimens used, that is, the existence or non-existence of backing strip. Typical load-tip deflection curves at the initial and steady states, defined as the state at about 20 % of the lives, are shown in Fig. 9.

b) Local Strain Behaviors

Typical relations between the strains of the flange at or near the beam end and the corresponding bending moments are graphically shown in Figs. 10～12.

In the case of specimens belonging to Series 1, strains at the beam end behave

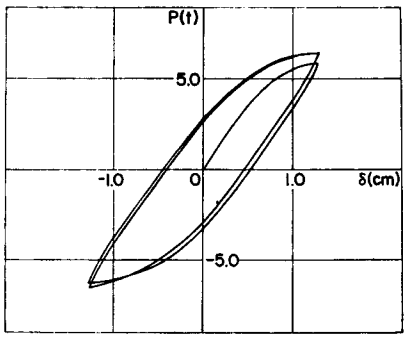

(9-a)

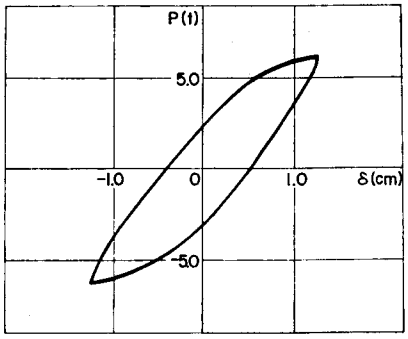

(9-b)

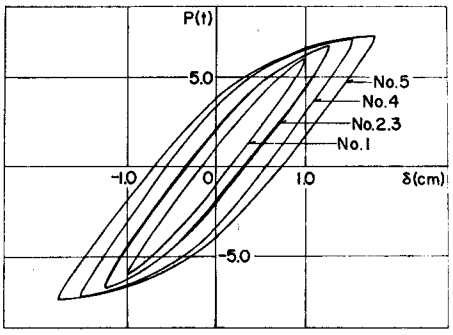

(9-c)

Fig. 9 (a)-Typical Load-Tip Deflection Relation of the Initial State of Series 1 ($\delta = \pm 1.26$ cm)
(b)-Typical Load-Tip Deflection Relation of the Steady tate of Series 1 ($\delta = \pm 1.26$ cm)
(c)-Load-Tip Deflection Relations of the Steady States of Series 2

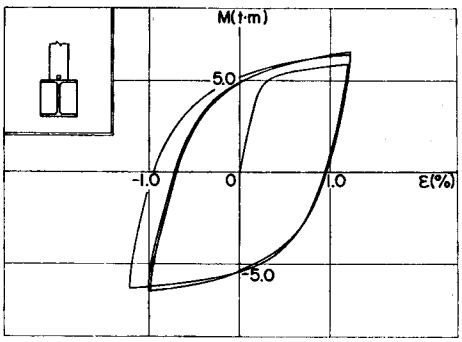

(10-a)

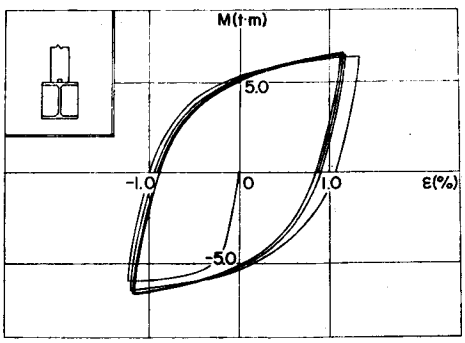

(10-a')

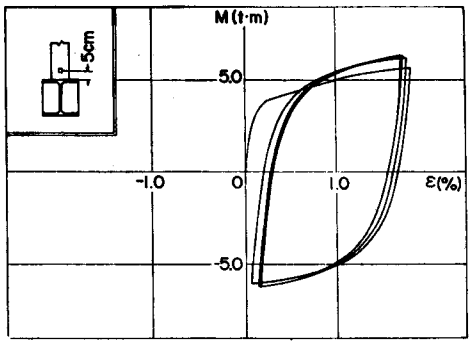

(10-b)

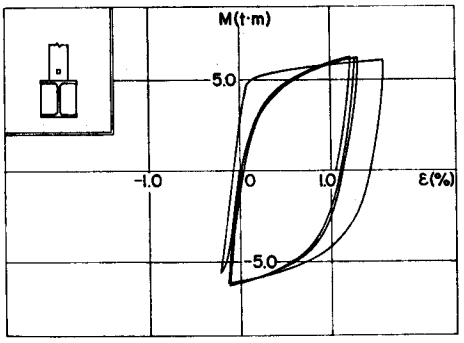

(10-b′)

Fig. 10 Moment-Local Strain Curves of Series 1($\delta = \pm 1.26$ cm)

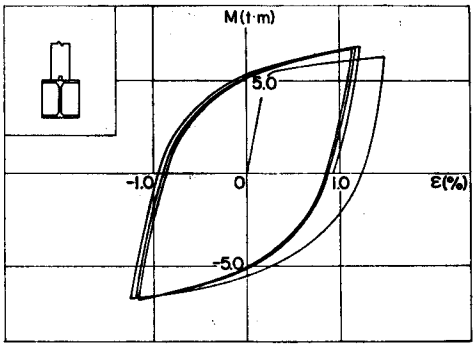

(11-a)

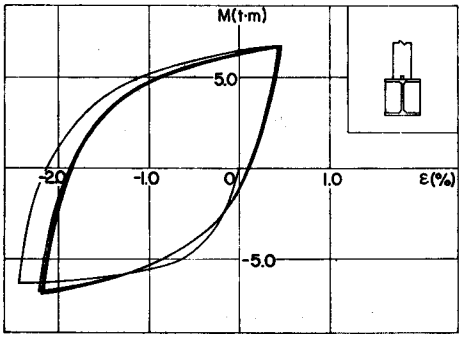

(11-a′)

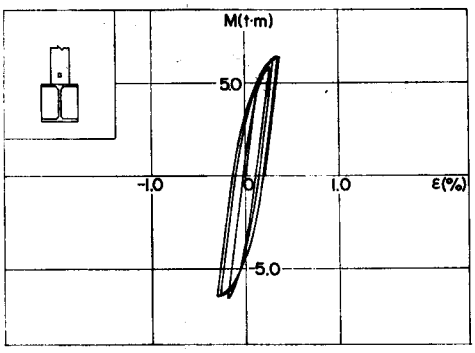

(11-b)

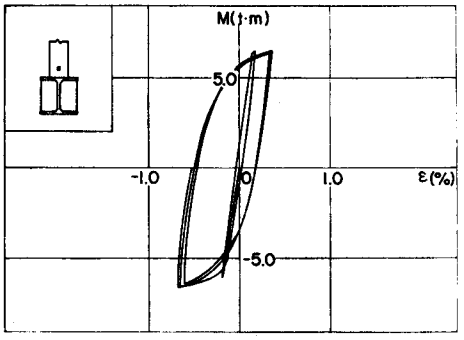

(11-b′)

Fig. 11 Moment-Local Strain Curves of Series 2($\delta = \pm 1.26$ cm)

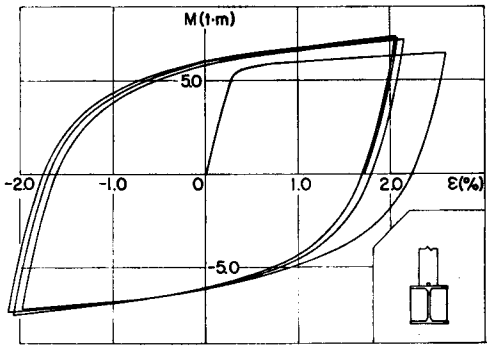

(12-a)

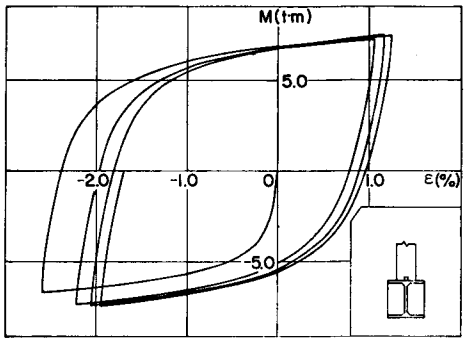

(12-a′)

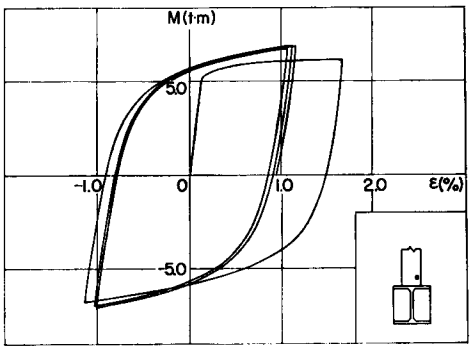

(12-b)

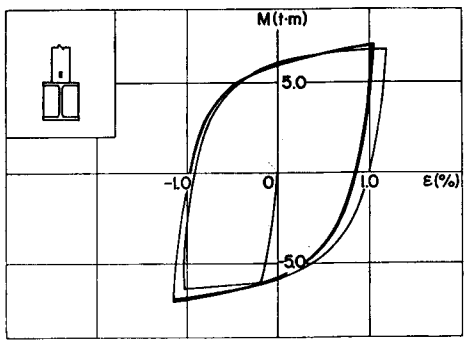

(12-b′)

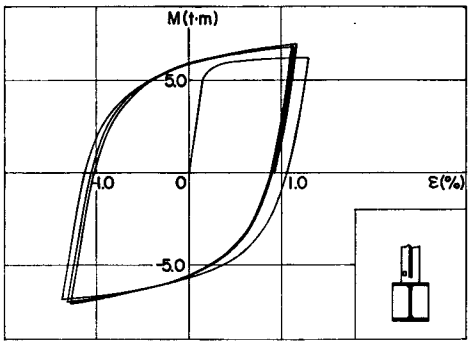

(12-c)

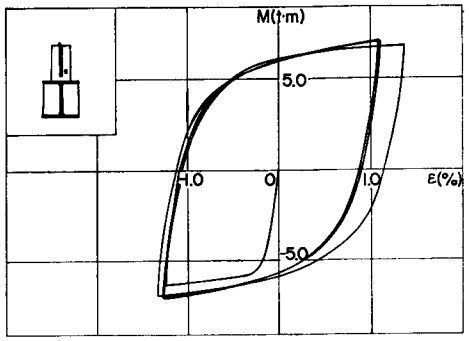

(12-c′)

Fig. 12 Moment-Local Strain Curves of Series 2($\delta = \pm 1.78$ cm)

with almost a zero mean strain. (See Fig. 10(a) and (a').) Strains measured at locations 5 cm apart from the beam end move toward the tension side, regardless of wheter the initial loading direction initiates from the tension side or compression side, as shown in Fig. 10(b) and(b').

From these results, it may be considered that there exists a tensile residual strain at the flange location 5 cm from the beam end. The backing strip welded to the beam flange acts as a stiffener, and the magnitude of the thermal strain due to welding is lessened. For this reason, the tensile residual strain generated by the flange shrinkage due to the weld heating cycle, concentrates on the beam flange areas adjacent to the stiffenend zone.

On the contrary, in the case of the specimens of Series 2, it can be considered that the tensile residual strain due to welding distributes uniformly along the beam flange at the beam end, because of the absence of the backing strip. This is evident from the result of the strain behavior at or near the beam end, as shown in Figs. 11 and 12. The so-called Bauschinger effect can be distinctly observed at the flange of the beam end when the loading starts from the compression side. (See Figs. 11(a') and 12(a').) Such an effect is not observed when the loading begin from the tension side. (See Figs. 11(a) and 12(a).)

The moment-strain relations at locations 5 cm from the beam end show a symme -tric shape with respect to the origin. Hence, it can be supposed that the residual strain due to welding has been weakened and diminished at this location, as shown in Fig. 11(b) and(b'), and Fig. 12(b)$\sim$(c').

After the first or second cycle, the moment-strain relations inherently stabilize, though they are influenced by the initial loading directions, and are dependent upon the initial strain magnitude.

c) Strain Distribution Characteristics

Strain concentration phenomena can be frequently observed in steel structures. Such phenomena are often due to the fabrication process, namely scalloping and welding performances. Since they can occur at the beam end, a thorough study of its characteristics is much needed to account for the seismic safety of the beam-to-column welded joints. For this reason, Fujimoto et al[4] conducted investigations to clarify such strain concentration phenomena at or near the beam-to-column connections, using idealized beam-to-column welded joints consisting of ultra-thick column flange sections. However, their findings are not directly applicable to the actual welded beam-to-column connections, because they fail to consider such significant factors as the residual stresses (or strains) and the stiffening effects due to the diaphragms and the backing strips which have an influence upon the strain concentration phenomena.

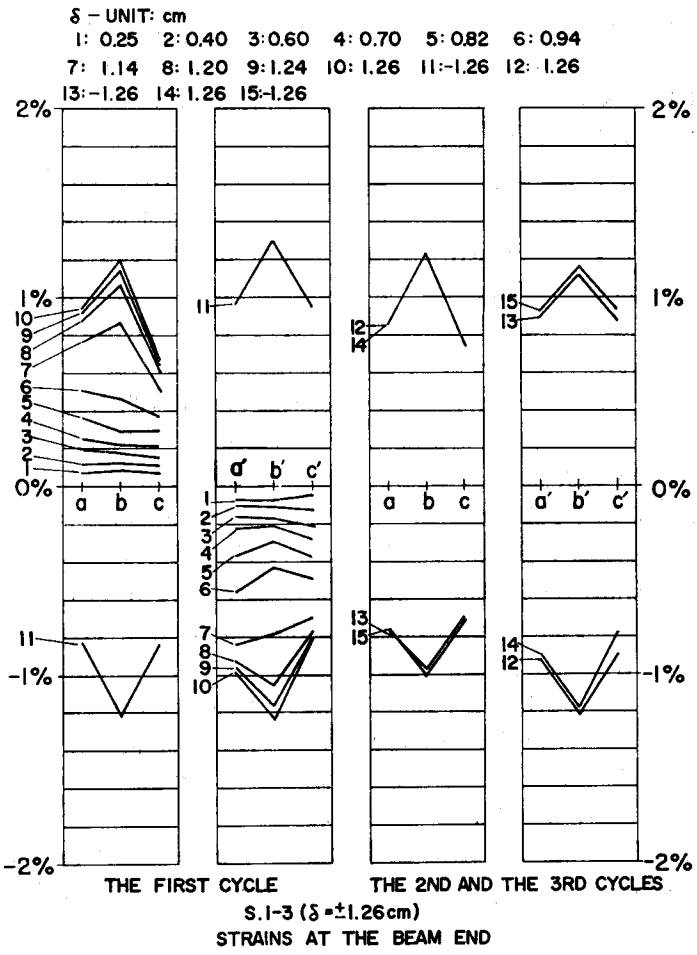

(13-a)

For this reason, in this paper, the discussions on strain distribution properties are limited to the qualitative aspects of such behavior.

i) Series 1

Fig. 13(a) shows the typical strain distributions at the beam end for Series 1-3 ($\delta = \pm 1.26$ cm). Symmetrical and convex distribution patterns are observed at the initial tension and compression sides, and are maintained unchanged in the subsequent cycles.

However, the strain distributions at a distance 5 cm apart from the beam end depend upon the initial loading direction of the flange, since they are directly affected by the residual strains due to welding, as shown in Fig. 13(b). That is, the distributions of the flange, where the initial loading starts from the tension side, show a

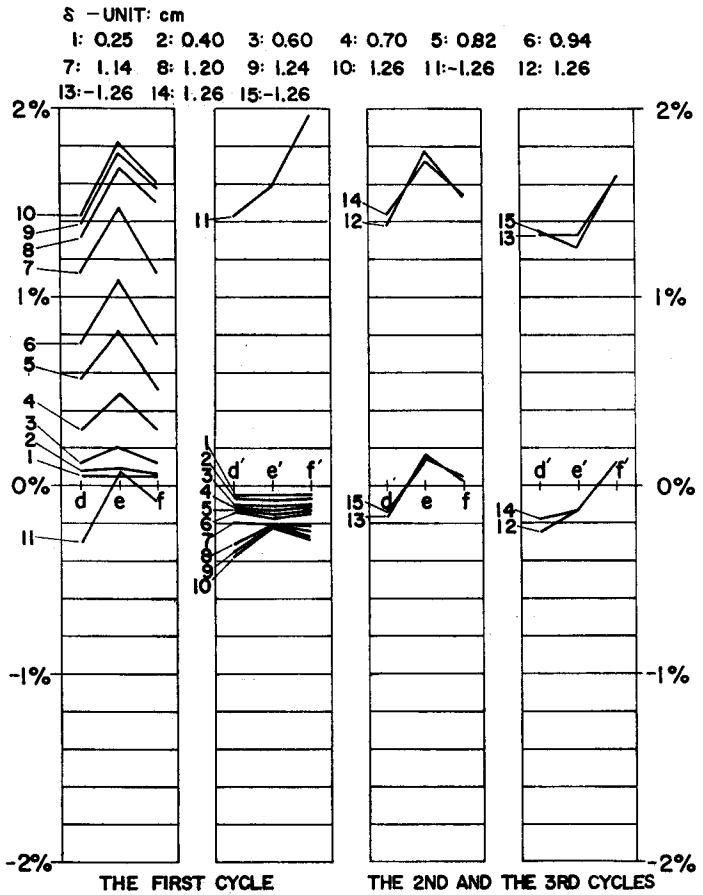

(13-b)

Fig. 13 Strain Distributions of Series 1($\delta = \pm 1.26$ cm)

convex pattern at the tension side. After this, at the next compression side, a concave pattern is observed This pattern continues without variation over the next few cycles with the distributions being convex at the tension sides and concave at the compression sides. That is, each local strain range is kept constant.

On the contrary, when the loading starts from the compression side in the flange concave patterns are exhibited in the first two excursions. However, in the subsequent cycles, the distribution patterns are convex at the compression sides and concave at the tension sides.

ii) Series 2

The strain distributions at the beam flange of Series 2 are somewhat different

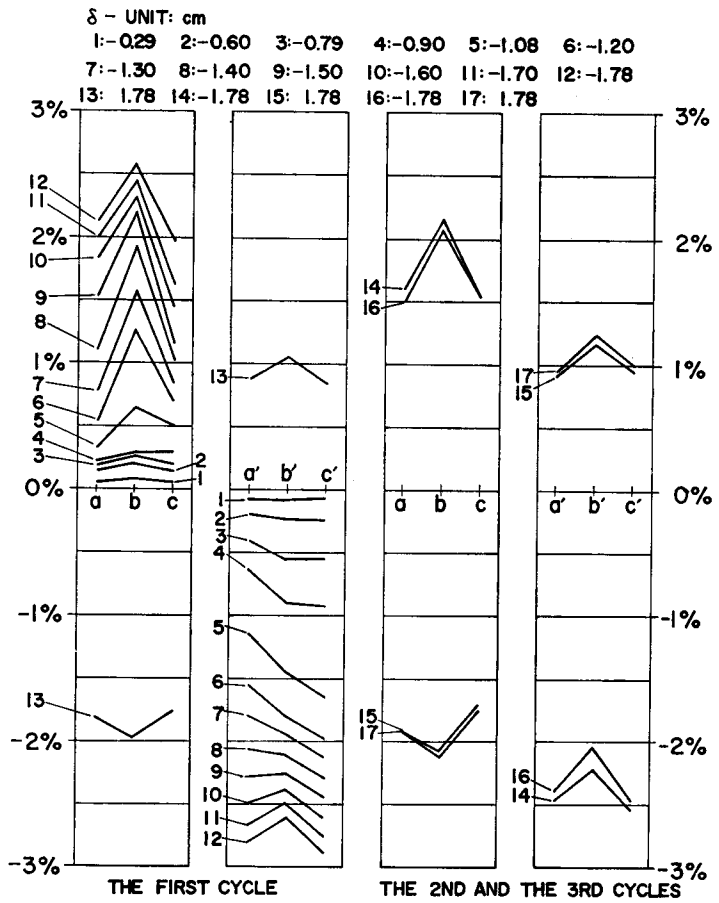

from those of Series 1. Convex patterns are observed at the initial few cycles independent of the loading directions in the case of comparatively small deflection amplitudes, namely, within about 1.26 cm. These phenomena are also found when the initial loadings start from the tension side, without regard to the magnitude of the deflection amplitudes.

When the flange is initially subjected to the compressive stress and its local strain values exceed -2.0 %, the strain distribution patterns become concave.

However, after unloading, at the instant when the flange reaches its peak tensile loading, the distribution pattern returns to its original convex form. Even after the next few cycles, these patterns remain concave at the compression sides and convex at the tension sides. A typical example of such behavior is shown in Fig. 14(a).

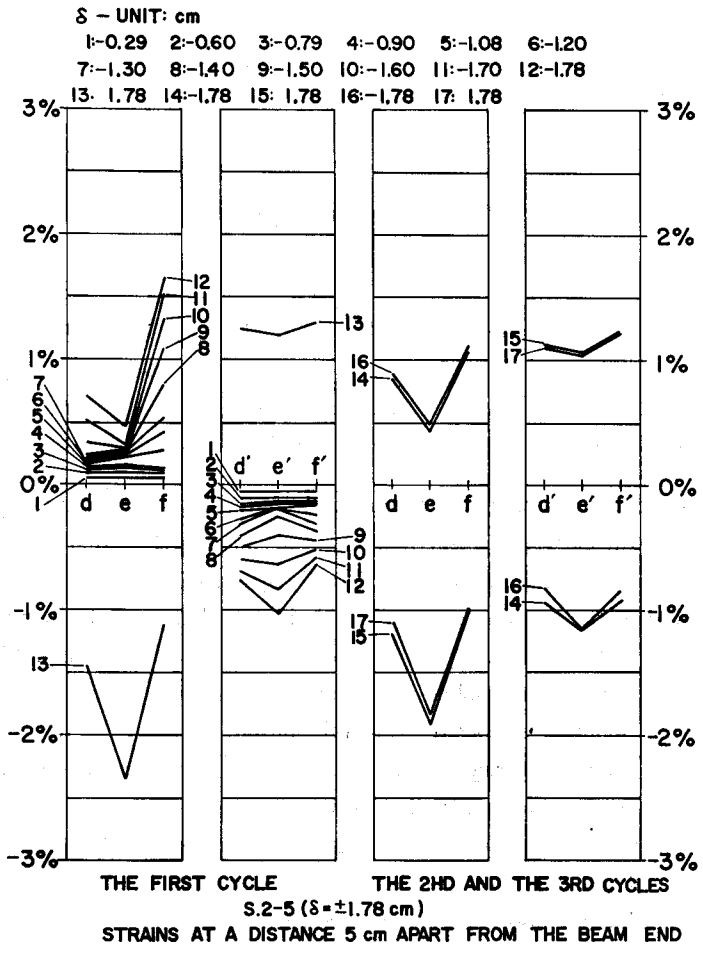

(14-b)

Fig. 14 Strain Distributions of of Series 2($\delta = \pm 1.78$ cm)

The typical strain distributions at a distance 5 cm apart from the beam end are shown in Fig. 14(b). The patterns are contrary to those at the beam end, since the strains are affected by the end actions of the beam flange.

4. Low Cycle Fatigue Strength

4.1 Determination of Strain Values

Strain values along the flange width at the beam end are not necessarily constant, and in some cases are distinctly influenced by the loading directions at the initial states, as described in Section 3. Moreover, as the quantitative estimates of these characteristics lie beyond the scope of this paper, the absolute values of the six strain

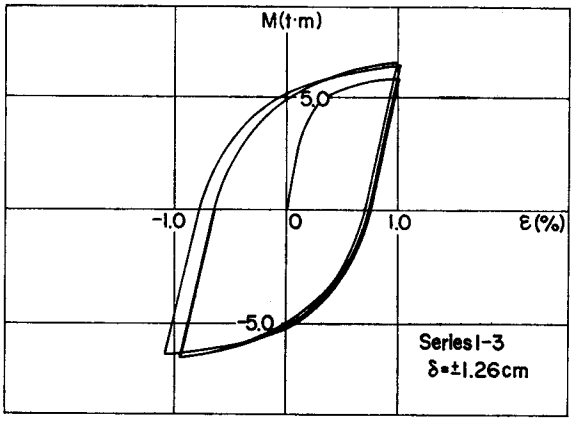

Fig. 15 Moment-Average Strain Curves of Series 1($\delta=\pm 1.26$ cm)

values at the same cross-section were averaged and used to account for the fatigue strength at the beam end. This method may be adequately applied in the case of Series 1, since the local strain values are virtually symmetrical for the stiffening effect of the flange due to the backing strip. The relationship between the bending moment versus the averaged strain of the specimens of Series 1 is shown in Fig. 15.

The same procedure was applied with respect to the results of Series 2. Fig. 16 shows the bending moment-averaged strain relationship. From the figure, it is noted that the bending moment-averaged strain curves are unsymmetrical with regard to the vertical axis, namely, the compressive average strains exist.

Several investigators have discussed the effect of average strain in estimating the fatigue strength. Recently, some investigations[8),9)] have reported that not only the tensile average strain, but also the compressive strain produces a drop in the fatigue

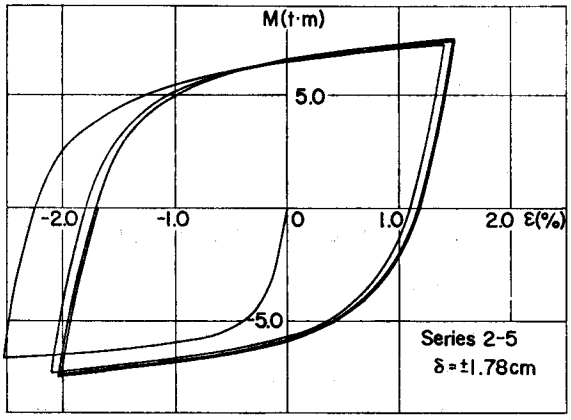

Fig. 16 Moment-Average Strain Curves of Series 2($\delta=\pm 1.78$ cm)

strength, in comparison with the fatigue strengths obtained from the perfectly symmetrical strain control tests.

In the present experiment, however, the influence of the average strain is not taken into consideration, as may seem advisable, for the following reasons.

As the compressive average strain is caused by the thermal alteration due to the welding which induces the strain of beam flange to exceed its elastic range, it may be necessary to determine accurately the stress-strain relations of the material, in order to predict the average strain. However, the present test result may be inadequate for determining the residual strain due to the welding calculated from the virgin stress-strain relation. Moreover, for our present purposes, it may be reasonable to not consider the influence of the residual strain, because of the incorporation of the averaged strain calculated by using the tensile and the compressive strains.

4.2 Non-dimensional Strains

Since the mechanical properties of the materials are different from each other, as shown in Table 1, their influence upon the fatigue strength must be taken into consideration. From this point of view, it is desirable to represent the strain amplitudes (or ranges) in the nondimensional form, instead of the measured dimensional strains. This idea and its procedure have already been proposed elsewhere (Ref. 7).

However, the yield strains obtained from material testing are not directly applicable as experimental data, because the basic mechanical properties have been affected and changed by the thermal alteration due to welding. For this reason, assuming that the initial stiffeness remains unchanged until the point at which the beam end arrives at the fully plastic moment, M_p, then the corresponding plastic strain, ε_p, can be computed using the relation, $M_p/\varepsilon_p = M_y/\varepsilon_y$. Through these approximations, the non-dimensional elastic and plastic strain ranges can be obtained by dividing the averaged strain ranges by the plastic strain, ε_p.

4.3 Estimate of Fatigue Strength

The non-dimensional strain rates, $\Delta\varepsilon_e/\varepsilon_p$ and $\Delta\varepsilon_e/\varepsilon_p$, versus the corresponding fatigue lives, N_f, were plotted on a log-log scale. The results are shown in Fig. 17. Since no distinct differences between the data of Series 1 and 2 can be observed in this figure, the method of least squares was employed for all plotted data, and the following equations were obtained:

$$\begin{aligned} \Delta\varepsilon_e/\varepsilon_p &= 5.3 \cdot (N_f)^{-0.17} \\ \Delta\varepsilon_p/\varepsilon_p &= 103 \cdot (N_f)^{-0.59} \end{aligned} \qquad (1)$$

These formula are also represented in the figure. by the straight lines.

By the application of the crack initiation lives, N_c, in the place of N_f, other linear

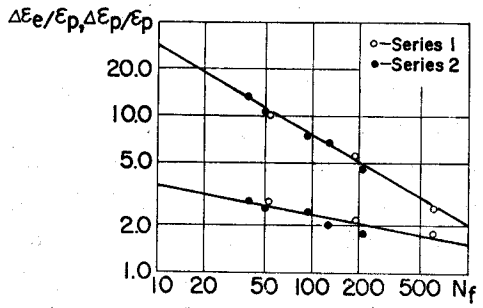

Fig. 17 Relations between the Non-dimensional Strain Ranges and the Fatigue Lives

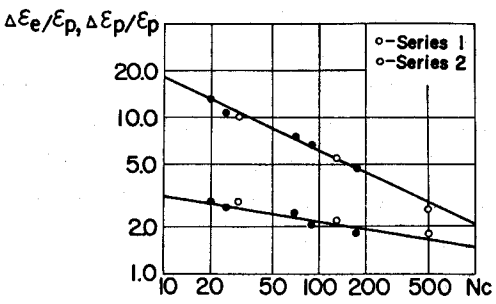

Fig. 18 Relations between the Non-dimensional Strain Ranges and the Crack Initiation Lives

relations were formulated and compared with Eq. (1). The formulas can be equated as follows:

$$\Delta\varepsilon_a/\varepsilon_p = 4.5 \cdot (N_c)^{-0.16}$$
$$\Delta\varepsilon_p/\varepsilon_p = 53.4 \cdot (N_c)^{-0.47} \qquad (2)$$

The experimental data and the regression lines are shown in Fig. 18.

The fatigue strength for mild steel has already been formulated by Tanabashi et al[5] and Hanai et al[6], from the test results using the flange plates of JIS SS 41 wide flange sections. The authors[7] have also reported the fatigue strength properties for several base metals, mild to high tensile steel, and welded joints.

Even though the comparison of the aforementioned results[5)~7)] with those obtained from this experiment may not be precise, because of the differences in strain distribution properties due to the specimen shapes, it may be considered to be a rough estimate of the application limits of the results obtained from the material tests. The results of the fatigue strength are reformulated from Refs. (5) and (7), as follows:

From Ref. (5)

$$\Delta\varepsilon_p = 0.38 \cdot (N_c)^{-0.53}$$

in the non-dimensional form,

$$\Delta\varepsilon_p/\varepsilon_y = 280 \cdot (N_c)^{-0.53} \qquad (3)$$

From Ref. (7)

for the base metal of SS 41:

$$\Delta\varepsilon_a/\varepsilon_y = 440 \cdot (N_{ft})^{-0.58} + 5.2 \cdot (N_{ft})^{-0.10}$$

for the weld metal:

$$\Delta\varepsilon_a/\varepsilon_y = 480 \cdot (N_{ft})^{-0.63} + 6.2 \cdot (N_{ft})^{-0.16} \qquad (4)$$

for the H. A. Z.:

$$\Delta\varepsilon_a/\varepsilon_y = 680 \cdot (N_{f'})^{-0.68} + 8.0 \cdot (N_{f'})^{-0.17}$$

where $N_{f'}$: equivalent fatigue life which is obtained by dividing the total dissipated plastic strain energy to failure by the plastic strain energy per cycle at the steady-state.

From the comparison of Eqs. (1) and (2) with Eqs. (3) and (4), each corresponding exponent may seem unremarkable with respect to the difference of the specimen shapes. However, the coefficients are remarkably different from each other, that is, the coefficients obtained for Eqs. (3) and (4) are four to five times those of Eqs. (1) and (2).

Such a consideration may lead to a general interpretation of the fatigue strength of the actual beam-to-column connections, which is arrived at by multiplying a reduction factor by the coefficients of the fatigue strength equations obtained from the material tests.

5. Discussions and Conclusions

Welded beam-to-column connections consisting of rolled wide flange sections were tested to examine the moment-strain behavior at the beam ends and low cycle fatigue strength. The principal results observed from this experiment are as follows:

[1] Though the strains of the flange at the beam end are affected by thermal alteration due to welding, they constrict and stabilize into hysteretic loops during the first few cycles. Their behavior, however, is distinctly influenced according to whether or not the beam flanges are butt-welded with backing strips. The experimental results show that the backing strips stiffen the beam flanges. For this reason, the strains of the beam-to-column connections with backing strips are mitigated, and are symmetrical with respect to their origins.

[2] The averaged strain ranges were computed and used for the estimate of the fatigue strength. The relations between the lives to failure and the averaged strain ranges, as well as the crack initiation lives and the averaged strain ranges, were equated and compared with those obtained from the material tests. Though these simple comparisons do not consider the effect of the specimen shapes and the strain concentrations, it is possible to approximate the fatigue strength of the actual welded beam-to-column connections from the results of the material test, by a modification of the resultant coefficients of the latter.

References

1) S. Igarashi; Aseismic Safety of Building, A. I. J. Kinki Branch, p. 181 (1977)

2) E. P. Popov and V. V. Bertero; Proc. of A. S. C. E., ST 6, June, p. 1189, (1973)
3) A. I. J.; Seismic Loads and Aseismic Safety of Building, p. 615 (1976)
4) M. Fujimoto, et al; Trans. of A. I. J., No. 245, July, p. 63 (1976), No. 264, Feb., p. 73 (1978), Jan., p. 1 (1979) and No. 276, Feb., p. 27 (1979)
5) R. Tanabashi et al; Trans. of A. I. J., No. 175, Sept., p. 17 (1970) and No. 176, Oct., p. 25 (1970)
6) M. Hanai et al; Trans. of A. I. J., No. 184, June, p. 29 (1971)
7) K. Kaneta and I. Kohzu; THIS MEMOIRS, Vol. XLIII, part 1, Jan., p. 102, (1981)
8) K. Iida; Metals in Engineering, 8, No. 3, p. 11 (1968)
9) K. Ohji, W. R. Miller and J. Marin; J. of Basic Eng., Dec., 1966